PyLRO: A Python calculator for analyzing long-range structural order

Kevin Parrish,[1,a] (iD) Qingyang Hu,[2,b] (iD) and Qiang Zhu[3,c] (iD)

AFFILIATIONS

[1]Department of Physics and Astronomy, University of Nevada, Las Vegas, Nevada 89154, USA
[2]Center for High Pressure Science and Technology Advanced Research, Beijing 100193, China
[3]Department of Mechanical Engineering and Engineering Science, University of North Carolina at Charlotte, Charlotte, North Carolina 28223, USA

[a]Electronic mail: parrik1@unlv.nevada.edu
[b]Electronic mail: qingyang.hu@hpstar.ac.cn
[c]Author to whom correspondence should be addressed: qzhu8@charlotte.edu

ABSTRACT

We present PyLRO, an open-source Python calculator designed to detect, quantify, and display long-range order in periodic structures. The program's design methodology, workflow, and approach to order quantification are described and demonstrated using a simple toy model. Additionally, we apply PyLRO to a series of metastable $AlPO_4$ structural intermediates from a prior high-pressure study, demonstrating how to compute and visualize structural order in all directions on a Miller sphere. We further highlight the program's capabilities through a high-throughput analysis of structural patterns in the pressure-induced amorphization of $AlPO_4$, revealing atomistic insights into specific energy regions of massive amorphous structures. These results suggest that PyLRO can be a valuable tool for investigating crystal–amorphous transition in materials research.

I. INTRODUCTION

Broadly speaking, materials can be classified as crystalline, quasi-crystalline, and noncrystalline based on their atomic ordering. The long-range translational symmetries define the structure of crystalline materials and give rise to many fascinating properties for materials science.[1] Much of the crystallographic theory is built upon the concept of idealized, perfectly ordered crystals, which provides a framework for understanding symmetry-breaking phenomena. In contrast, noncrystalline solids, often referred to as amorphous solids, lack these long-range symmetries, leading to a much wider variety of material types. The challenge of identifying useful materials from the vast space of possible amorphous solids is formidable. Crystallographic theories, such as Zachariasen's random network theory for glass formation,[2] have been fairly successful in explaining amorphous solid formation by applying crystal chemistry rules and patterns. However, much remains to be explored, particularly concerning the extent to which some amorphous solids still conform to crystallographic principles of long-range order.

A deeper structural connection between crystalline and noncrystalline solids can be understood by examining the formation of noncrystalline solids through pressure-induced amorphization (PIA) processes. Amorphous materials produced via PIA are particularly interesting because, as disordered phases of originally perfectly ordered crystals, they offer a higher likelihood of being understood and engineered using a well-established crystallographic theory. The probability of applying crystallographic principles from perfect crystals to interpret these amorphous structures is greater, given their origin from crystalline phases. Though amorphous structures can be realized through other routes[3,4] and PIA does not necessarily promote amorphization,[5] it has been shown that internally consistent thermodynamic descriptions of this amorphization is possible.[6] Silica (SiO_2) is an archetypal material for the study of this phenomenon. The theory behind the reconstructive phase

transitions of SiO_2 polymorphs through pressurization is thoroughly explained by Dmitriev.[7] The study of SiO_2's amorphous forms is still of interest nowadays.[8] Recent research has investigated PIA created amorphous solids as potential intermediates in a crystal–crystal phase transition.[9] This introduces a fascinating avenue of study: formalizing an understanding of the topological long-range order in crystals that potentially survives in their amorphous phases.

An important distinction in discussing order within amorphous structures lies between short, medium, and long-range order. Short-range order (SRO) refers to the local consistencies on the smallest scale, typically between individual atomic species.[10,11] Medium-range order (MRO) extends beyond SRO, describing the structural organization of how local units connect and arrange themselves to fill three-dimensional space.[12] In this work, we are particularly interested in the long-range order (LRO) that represents the prototypical periodicity throughout the entire bulk of perfect crystals. Importantly, we aim to study the evolution of LRO in solids as a precursor to amorphous materials. An exaggerated example of this would be fullerene–carbon cages that exhibit LRO using amorphous building blocks.[13] Through pairwise distribution analysis, long-range ordering concepts, such as network topology, can be explored in glasses,[14] offering intriguing research possibilities. Recent work has also examined hidden topological ordering in PIA materials, shedding light on the connections between amorphous disorder and crystal orientation, further advancing theoretical foundations for LRO in non-crystalline solids.[15,16] Nevertheless, significant research is still required across various materials and simulations to deepen our understanding of these phenomena.

Herein, we present the program PyLRO, an open-source Python package built on top of Atomic Simulation Environment (ASE)[17] to quantify and visualize the relative LRO of solids. Using structure files of moderately sized supercells of an amorphous material, without any required dependency on a reference parent structure, PyLRO can streamline in-depth analysis of long-range periodicity in any arbitrary crystallographic direction. It provides intuitive quantification of order in each direction and displays the full projection of the structure's order on a crystallographic Miller sphere. We hope that this functionality can promote the study of topological order in amorphous materials by providing quick processing and visualization of computer-generated PIA structures during the amorphous–crystal transitions. In Secs. II and III, we will start with introducing the basis behind the order quantification as well as the program's workflow. Next, we will demonstrate its application to a set of $AlPO_4$ data, a quartz prototype with a well-studied PIA transition. Finally, we conclude with a discussion of the program's potential uses in other areas of materials research.

II. METHODOLOGY

A. Long-range order quantification

In this work, we aim to extract key structural information to quantify the long-range order of a supercell structure in an unbiased and efficient manner. For a PIA, the input structure should not rely on a crystalline reference, as this would limit the program's generality. Therefore, we seek to quantify LRO from only the atomic positions of a large supercell, without the use of the reference crystal.

To avoid the unit cell complexity, a representative species needs to be selected to capture the repeating unit, and the long-range order of the structure in each direction is assessed based on how closely the atomic spacings in each direction adhere to perfect periodicity. The task of quantifying the structure's order is thus reduced to measuring the degree of atomic displacement from an idealized "perfect" crystal. Once this displacement is quantified, projections of both the structure and its idealized form onto any set of Miller planes can be used to illustrate the relative long-range order.

To achieve this goal, we develop PyLRO by starting with fitting a crystalline sub-lattice to the input amorphous structure. Specifically, the program seeks to obtain an optimal lattice beneath the atoms of the structure by minimizing their displacements from ideal positions. The calculation driving this fit is analogous to the structure factor used in simulating x-ray diffraction. The structure factor S is defined as the squared modulus of the Fourier transform of the lattice, as expressed in Eq. (1),

$$S = \left| \sum_{i=1}^{n} e^{-2\pi i \mathbf{x_i} \cdot \mathbf{hkl}} \right|^2. \tag{1}$$

Traditionally, the structure factor is used to identify the directions in a crystal where scattering can produce non-zero intensity, making it a powerful tool for extracting periodicity characteristics. In our case, the atomic positions along the structure's basis directions are projected onto a multi-period grid of plane waves. The period that yields the largest magnitudes from these projections is used as a determination of the optimal number of repeating units along the basis directions.

In determining the supercell dimensions of the structure, care must be taken to select a fit that maximizes the d-spacing along the basis directions. For instance, a structure with three repeating units along a direction would produce similar scattering results from a wave with a three or six period. However, it would be incorrect to calculate disorder based on six repeating units, so the smallest possible multiple is always selected. Overall, we found that the confidence in PyLRO's ability to fit a crystalline sublattice to PIA structures is particularly high for those close to their crystalline phase. Nevertheless, this should not apply to study structures nearing complete disorder, where atomic displacements become so irregular that any quantified order would be negligible. Identifying the best possible crystalline sublattice is crucial, as disorder is primarily measured by the displacement of atoms relative to this calculated reference lattice.

After identifying an optimal sublattice reference, the next step is to calculate the precise displacements of each atom in the amorphous structure. By scaling the atomic positions to approximate their integer coordinates within the supercell, the displacements from these integer values can be understood as the fraction of a full period (or d-spacing) that the atoms deviate in any given direction. To quantify long-range order along any Miller plane, we measure the average deviation of each atom from its ideal lattice point, expressed as a percentage of the lattice spacing in

that specific direction. This allows for a consistent comparison of disorders across different directions, independent of the actual lattice spacing. Projections onto non-basis directions are always evaluated relative to the corresponding projection of the crystalline sublattice, which serves as the reference point for comparison.

Figure 1 illustrates this design philosophy by quantifying the LRO of a simple two-dimensional toy model. In Fig. 1(a), the red points represent the atomic locations of the species selected to represent the repeating unit. The model demonstrates how significant amorphous deviations can cause atoms located near the boundary (due to periodic boundary conditions) to be displaced across to the opposite side of the supercell. Despite these minor deviations, the presence of long-range order in the structure is still evident and can be detected and quantified. Figure 1(a) also highlights how the calculated structure factor S values for multiple periods help identify the lattice dimensions through periodic boundaries, without any prior knowledge of the reference crystal. Clear peaks are visible at eight along the a-axis and at five along the b-axis. With these dimensions, PyLRO fits a lattice to the structure by (i) multiplying the atomic coordinates with the integer dimensions (ℓ), (ii) detects the ideal sublattice values (m) by rounding the coordinates to the nearest integers, and (iii) computes the atomic disorder from the displacement between ℓ and m. Finally, whole structural disorder ($\bar{d}$) can be determined by taking the average of atomic disorder values (d). The entire procedure is also listed in the table of Fig. 1(b).

It is worth addressing two points for clarity. The first is that, while this toy model has simple axes at right angles, the program is generalizable to more complex systems. PyLRO is built on top of the structural functionalities of ASE, which can provide atomic positions scaled relative to arbitrary cells defined in the input structure file. This allows analysis of each crystallographic direction independently even for non-orthorhombic systems.

The second is the distinct difference between the structure factor and the calculated value for structural disorder. The ability of Eq. (1) to detect periodicity is used as a robust way to detect periodic clustering of scaled atomic positions around potential lattice points. The exact value of S itself can be understood as the collective drop in magnitudes of points along a complex exponential as they deviate away from peaks, a definition that does not have much intuitive meaning for disorder and has non-linear scaling. This is why PyLRO uses the shape of the structure found through S maximization to fit a sublattice and calculates disorder as percent deviation of lattice spacings.

B. Miller sphere plot

In addition to quantifying order, we are also interested in visualizing the overall long-range order of the entire amorphous structure graphically. To achieve this, PyLRO includes plotting functionality that generates a 3D Miller sphere—a unit sphere on a 3D plane defined by the **a**, **b**, and **c** basis vectors of the structure. Each point on the surface of the sphere corresponds to a specific Miller plane. Following the coauthor's recent work,[18] we use a series of Fibonacci points to provide an approximately equal distribution of points across the sphere's surface, ensuring uniform sampling of directions.
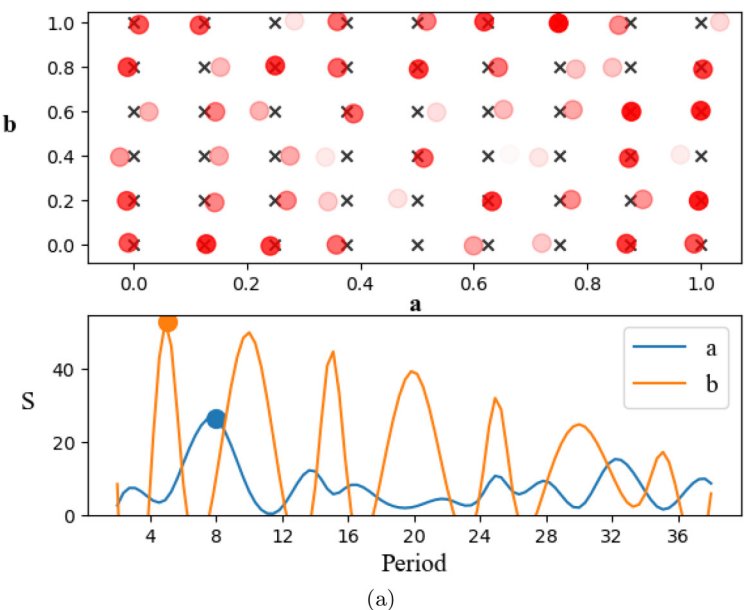
Atom Location	Sublattice Fit ℓ	Lattice Point m	Disorder d
n (x, y)	(cx, dy)	round(ℓ)	$|m - \ell|$
0 [-0.01, 0.01]	[-0.08, 0.05]	[0, 0]	[0.08, 0.05]
2 [0.24, 0.0]	[1.92, 0.0]	[2, 0]	[0.08, 0.0]
4 [0.46, 0.01]	[3.68, 0.05]	[4, 0]	[0.32, 0.05]
6 [0.72, 0.01]	[5.76, 0.05]	[6, 0]	[0.24, 0.05]
8 [0.99, 0.01]	[7.92, 0.05]	[8, 0]	[0.08, 0.05]
10 [0.14, 0.19]	[1.12, 0.95]	[1, 1]	[0.12, 0.05]
12 [0.34, 0.2]	[2.72, 1.0]	[3, 1]	[0.28, 0.0]
14 [0.63, 0.2]	[5.04, 1.0]	[5, 1]	[0.04, 0.0]
16 [0.9, 0.21]	[7.2, 1.05]	[7, 1]	[0.2, 0.05]
$\vdots$			
38 [0.25, 0.81]	[2.0, 4.05]	[2, 4]	[0.0, 0.05]
40 [0.5, 0.79]	[4.0, 3.95]	[4, 4]	[0.0, 0.05]
42 [0.78, 0.79]	[6.24, 3.95]	[6, 4]	[0.24, 0.05]
44 [1.0, 0.79]	[8.0, 3.95]	[8, 4]	[0.0, 0.05]
46 [0.12, 0.99]	[0.96, 4.95]	[1, 5]	[0.04, 0.05]
48 [0.36, 1.01]	[2.88, 5.05]	[3, 5]	[0.12, 0.05]
50 [0.62, 1.01]	[4.96, 5.05]	[5, 5]	[0.04, 0.05]
52 [0.86, 0.99]	[6.88, 4.95]	[7, 5]	[0.12, 0.05]

Average Disorder: $\bar{\mathbf{d}}=(0.14, 0.03)$

(a)   (b)

FIG. 1. A toy model of a partially disordered structure with exaggerated disorder along the crystallographic a-axis. The left panel (a) demonstrates the evolution of structure factor S as a function of period. The reference supercell dimension can thus be derived from S. The right panel (b) illustrates the procedures that quantify structural order based on the atomic deviations with respect to the reference unit cell.

For each point on the sphere, PyLRO calculates the long-range order parameter for the corresponding Miller plane and adds a Gaussian function scaled to $1 - O_{hkl}$, where O_{hkl} represents the calculated order parameter for the hkl plane. After normalization, the resulting figure warps the surface of the sphere to visually highlight the crystallographic directions with the highest long-range order. This visualization allows for a clear and intuitive understanding of the structure's directional order, with the deformations of the sphere indicating regions of stronger or weaker order within the amorphous material.

An associated adjustable color map further enhances the visualization by clarifying the most ordered directions, with a contour overlay on the sphere's surface to indicate regions of interest. Additionally, adjustable hyperparameters allow users to exaggerate or diminish the contrast between directions with strong and weak long-range order. These parameters can also control the sharpness of the peaks, making them more or less defined, depending on the desired level of detail. An example of this Miller sphere plot, including these features, will be discussed in Sec. III, demonstrating how the adjustable color map and hyperparameters help to distinguish and visualize the structure's directional order more effectively.

C. Workflow

The final demonstration of the program's workflow is shown in Fig. 2. In short, the process begins by loading an ASE-compatible structure file,[17] which represents a supercell of a partially disordered structure. The program then automatically detects the optimal sublattice beneath the structure using the theory described earlier. Once the sublattice is established, calculations of the average disorder in any given plane, or the identification of the most (or least) disordered global plane, can be performed. Finally, the program generates a visual diagram of the

FIG. 2. An overview of the PyLRO workflow.

structure's global order through a Miller sphere plot, offering an intuitive way to visualize the directional order.

The core of the order quantification logic focuses on identifying the ideal sublattice for the amorphous structure. Once this reference is established, fundamental principles of crystal periodicity are applied to measure atomic displacements and deviations in any direction. The plotting functionality leverages the complete quantification of disorder across all planes, enabling users to easily compare the relative long-range order between different directions. This workflow not only automates the key steps in quantifying the structural order but also provides clear visual representations to facilitate deeper insights into the degree of order and disorder within amorphous systems.

III. RESULTS AND DISCUSSIONS

$AlPO_4$ is an archetypal memory glass material for this kind of study. It has had many of its properties already thoroughly outlined in the literature, such as its vibrational modes,[20] pressure-induced transitions,[21,22] and potential memory glass effects.[23–25] In a recent analysis into topological ordering of memory glass on extended time scales,[15] an exploration of the $AlPO_4$ energy landscape under pressure found a **S**warm of highly probable **L**ow **S**ymmetry (SLS) structures connecting the high pressure phase of berlinite to the global minimum $AlPO_4$ II. In Sec. III A, we analyze the structures in this SLS using PyLRO to validate the function's accuracy against the current accepted theory around $AlPO_4$'s long-range topological order.

A. Case study on a sample structure

We begin with a sample structure. Figure 3(a) shows the aluminum substructure from three views. The projections onto the **ab** and **bc** planes show through visual inspection the degree to which the Al atoms deviate from the ideal crystal. While there is not much to choose from between the **a** and **b** directions, it is clearly seen that the **c** direction contains quite significant order. This is consistent with the calculated order parameters in each crystallographic basis direction, where **c** has the lowest disorder at 0.084. The average percent deviation of the atoms in the **c** direction is just 8.4% of the [001] d spacing.

Figure 3(b) captures this information and further analyzes a complete description of the structure's order in all directions. It shows that most ordered directions globally are a ring of planes around the miller surface with the **c** being most ordered basis direction. These directions in real space can be found through their products with the structure's basis matrix. The ring-like ellipsoid makes theoretical sense. The highest ordered directions should be perpendicular to the lowest order direction as the directions of maximum atomic deviations have been projected out. We would also expect a smooth plot because the contribution of any directional disorder should change continuously as the analysis window moves across directions where it is sampled more or less.

These results agree with and formalizes further the community acceptance of $AlPO_4$'s amorphous transition pathways. It was found by Zhu and co-workers[15] that the ideal description to understand amorphous $AlPO_4$ is that of an extreme Carpenter-type crystalline transition[26] as its signature memory glass effects rely on the
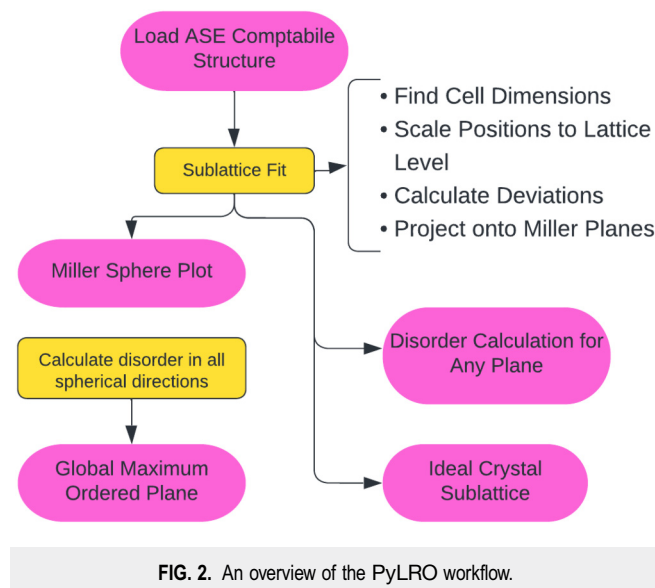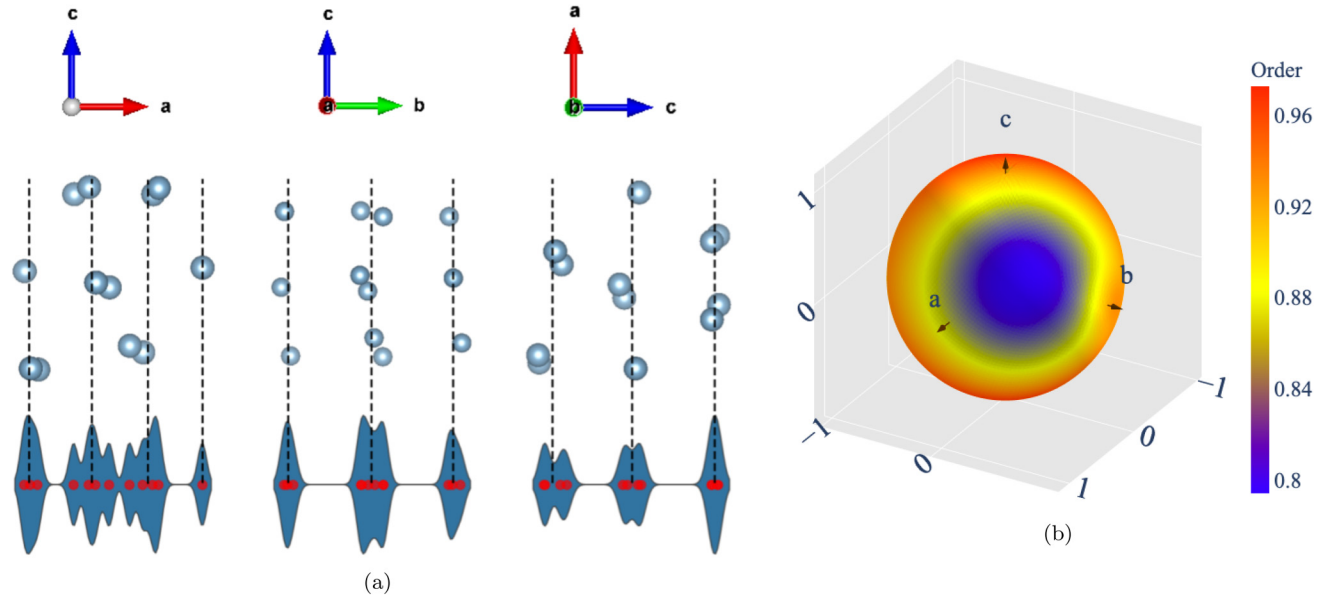
FIG. 3. (a) Aluminum sublattice in the sample $AlPO_4$ structure visualized by the VESTA software[19] in three basis directions. The violin plots demonstrate the degree of deviation of the atoms from their respective sublattice positions. The calculated disorders are 0.145 along **a**, 0.112 along **b**, and 0.084 along **c**. (b) The associated Miller sphere plot for all directions, suggesting that of the basis direction, **c** exhibits the maximum order while a direction close to the **ab** plane ([0.665, 0.602, 0.441]) possesses the minimum order.

long-range order that survives as crystal $AlPO_4$ II deforms topologically, the relatively low energy barrier heights of which can be through the integral of spontaneous strains from Carpenter's theory.[27] Transition pathway analysis showed that while the medium-range order describing the relative orientation of the characteristic Al-/P- polyhedra was broken, the short-range order of the polyhedra structures was kept mostly intact and the long-range order is partially kept. Figure 3(b) shows that the **c** direction of the chosen representative structure of the SLS retains a healthy amount of long-range order, preserving the connectivity of the structure's building blocks along that direction. Further, **a** and **b** being disordered in relatively equal amounts supports the current understanding of $AlPO_4$'s spiral ring symmetries during amorphization: the long-range symmetry in the **c** direction remains topologically strong as the symmetries within the rings in the **ab** plane break down. We can analyze these results through the lens of a ringed spiral structure for additional insight. The "backbone" of such a structure should be the even spacing of polyhedral rings along the spiral **c**. For it to deform topologically, it makes sense the rings should not deviate far in this direction as losing this particular long-range order would mean polyhedra are no longer structured as a chain, making it unlikely to retain its crystalline "memory." The results verify that this long-range order of this disordered structure is strong relative to the ring plane, agreeing with this logic.

B. High-throughput analysis on a massive dataset

One of the primary benefits of PyLRO is its lightweight, allowing for high-throughput calculations on structure sets that

would otherwise be Figure 4(a) shows the density of states for the SLS created using 9533 structures from the coauthor's previous study.[15] Knowing the global minimum $AlPO_4$ II, we can do disorder analysis on amorphous structure in the higher energy ranges to identify patterns in the topological order as symmetries get broken. Figure 4(b) shows Miller sphere plots of structures along a trajectory connecting $AlPO_4$ II to Berlinite. It can be seen that the $AlPO_4$ initially shows perfect symmetry. As we move up the energy landscape, we can see that disorder does not affect the structures randomly. The structures begin to lose translational symmetry along the **a** direction first. The disorder manifests more so in the **b** direction further, and the order in the **c** direction throughout the entire trajectory remains strong and clearly better than that of **a** and **b**.

Furthermore, Fig. 5 provides a broader analysis of the average directional disorder across the entire energy landscape. The average disorder in the **a**, **b**, and **c** directions is calculated for groups of structures within preceding 1 eV increments. All energy values are represented as a ratio of the energy range between $AlPO_4$ II and berlinite. The results clearly show that the average disorder increases in all directions as we move higher up the energy landscape. Notably, the **a** direction remains more disordered than the other basis directions up to approximately 0.8 eV, at which point the disorder in the **b** direction begins to match it. This observation is consistent with the Miller sphere plots in Fig. 4(b). As expected, the **c** direction remains the most ordered on average throughout the energy landscape, suggesting that long-range topological order is preserved within the amorphous structures.
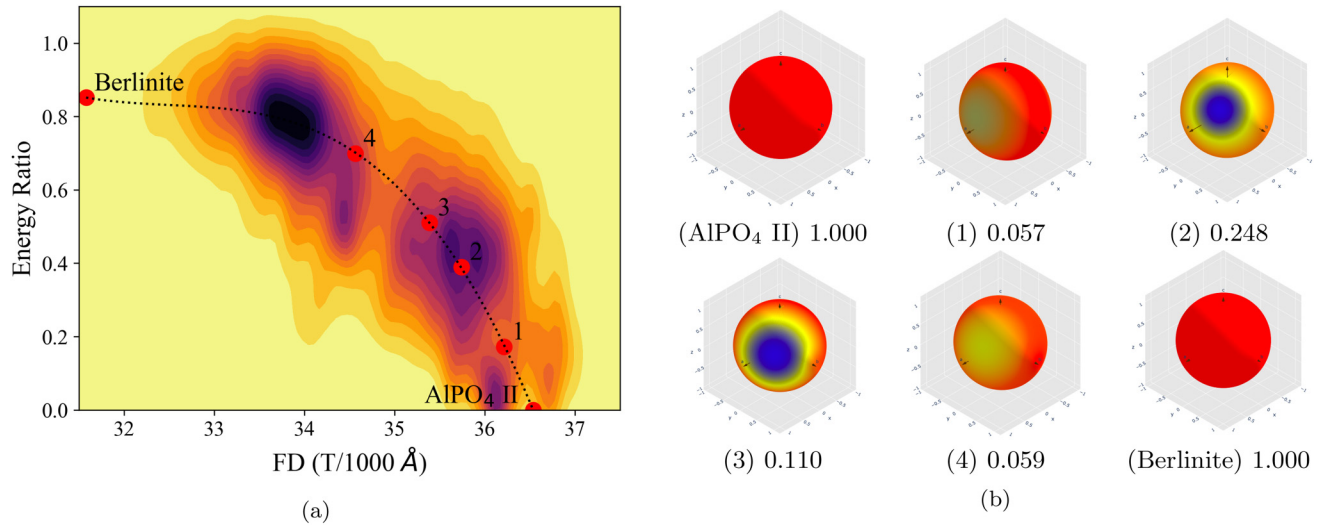
FIG. 4. (a) An energy landscape of the AlPO$_4$ SLS at 15 GPa against the structural framework density (FD). The high pressure of berlinite is toward the upper left, while the global minimum AlPO$_4$ II is at the bottom, both self labeled. (b) The evolution of Miller sphere plots of six representative structures along the transition trajectory from AlPO$_4$ II to berlinite. The values given are the average disorder among the basis directions.
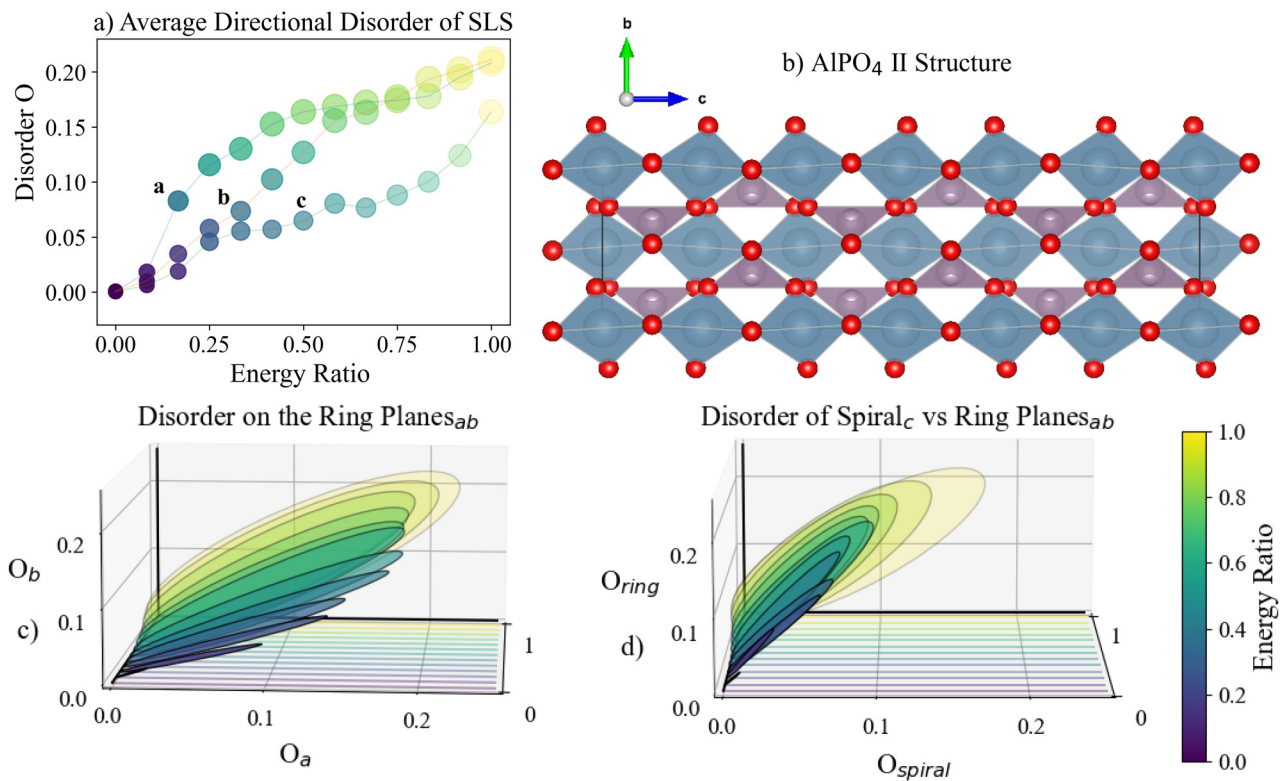

FIG. 5. (a) Plots the propagation of the averaged PyLRO calculated directional disorder of structures in regions of increasing energy in the SLS; (b) displays the crystalline AlPO$_4$'s spiraling polyhedra along the **c** direction; (c) displays a waterfall plot showing the evolution of disorder in the structures of the same regions between the directions of the ring plane **a** vs **b**; (d) is another waterfall plot showing the evolution of disorder between the spiral direction **c** vs planar disorder **ab**.

Using PyLRO, we can also conveniently visualize the anisotropic amorphization process in the two dimensional plane. Figures 5(c) and 5(d) present waterfall ellipse plots showing the evolution of disorder direction and magnitude within the ring plane of polyhedra, as well as the disorder along the topologically strong **c** direction relative to the average disorder in the ring plane. PyLRO's analysis across the energy landscape highlights how the topology of the structures changes. In the ring plane, the disorder in the **a** direction initially decreases the most. However, as disorder increases, it equalizes with that along the **b** direction. Interestingly, the disorder in the spiral **c** direction consistently remains lower than that of the **ab** ring plane, even as the overall disorder in the structures continues to increase.

Finally, the analysis reveals that independently calculated measures of the directions and magnitudes of maximum and minimum disorder (corresponding to the major and minor axes of the ellipse) are consistently perpendicular, as expected from symmetry considerations. This consistency further validates the accuracy of PyLRO in capturing both the magnitude and directional aspects of disorder within amorphous systems.

IV. CONCLUSION

The capabilities of the open-source Python package PyLRO, particularly its ability to calculate degrees of directional disorder, have been thoroughly demonstrated in this work. We provided detailed explanations of the program's workflow and design logic, illustrated through a simple amorphous model. For a rigorous test, we showcased PyLRO's performance using the well-studied material $AlPO_4$. By leveraging a large dataset of low-symmetry $AlPO_4$ structural intermediates, we demonstrated how PyLRO efficiently calculates and visualizes the degree of directional disorder for both individual structures and entire structure sets. Our analysis of a single sample revealed the long-range topological order that has been proposed as the underlying mechanism behind the structural memory effects in amorphous $AlPO_4$. Moreover, we showed how this long-range order can be rigorously quantified, matched with crystallographic intuition, and compared across different amorphous structures to provide a meaningful assessment of order and disorder.

Using PyLRO, we were able to perform a high-throughput analysis of a vast dataset comprising 9533 structures. This allowed us to gain insight into the pressure-induced amorphization of $AlPO_4$. Its utility extends to time-series data generated from molecular dynamics simulations or other advanced computational sampling methods. We believe that PyLRO will prove valuable to a wide range of researchers who are interested in studying the amorphous–crystal transition.

ACKNOWLEDGMENTS

AUTHOR DECLARATIONS

Conflict of Interest

The authors have no conflicts to disclose.

Author Contributions

Kevin Parrish: Formal analysis (equal); Methodology (equal); Software (equal); Validation (equal); Visualization (equal); Writing – original draft (equal); Writing – review & editing (equal). **Qingyang Hu:** Conceptualization (equal); Data curation (equal); Funding acquisition (equal); Validation (equal); Writing – review & editing (equal). **Qiang Zhu:** Conceptualization (equal); Formal analysis (equal); Funding acquisition (equal); Investigation (equal); Methodology (equal); Project administration (equal); Resources (equal); Supervision (equal); Validation (equal); Visualization (equal); Writing – original draft (equal); Writing – review & editing (equal).

DATA AVAILABILITY

The PyLRO source code, instructions, as well as scripts used to calculate the results of this study are available on Github at https://github.com/MaterSim/PyLRO, Ref. 28.

REFERENCES

[1] R. A. Evarestov, *Space Groups and Crystalline Structures* (Springer, Berlin, 2007), pp. 7–46.

[2] W. H. Zachariasen, J. Am. Chem. Soc. **54**, 3841 (1932).

[3] D. Turnbull, Contemp. Phys. **10**, 473 (1969).

[4] L. Zhong, J. Wang, L. Khoo, Z. Zhang, and S. Mao, Nature **512**, 177 (2014).

[5] S. J. Tracy, S. J. Turneaure, and T. S. Duffy, Sci. Adv. **6**, eabb3913 (2020).

[6] R. J. Hemley, A. P. Jephcoat, H. K. Mao, L. C. Ming, and M. H. Manghnani, Nature (London) **334**, 52 (1988).

[7] V. P. Dmitriev, P. Tolédano, V. I. Torgashev, and E. K. H. Salje, Phys. Rev. B **58**, 11911 (1998).

[8] H. Zhang, O. Tóth, X.-D. Liu, R. Bini, E. Gregoryanz, P. Dalladay-Simpson, S. De Panfilis, M. Santoro, F. A. Gorelli, and R. Martoňák, Proc. Natl. Acad. Sci. U.S.A. **117**, 8736 (2020).

[9] Y. Onodera, S. Kohara, P. S. Salmon, A. Hirata, N. Nishiyama, S. Kitani, A. Zeidler, M. Shiga, A. Masuno, H. Inoue, S. Tahara, A. Polidori, H. E. Fischer, T. Mori, S. Kojima, H. Kawaji, A. I. Kolesnikov, M. B. Stone, M. G. Tucker, M. T. McDonnell, A. C. Hannon, Y. Hiraoka, I. Obayashi, T. Nakamura, J. Akola, Y. Fujii, K. Ohara, T. Taniguchi, and O. Sakata, npg Asia Mater. **12**, 85 (2020).

[10] X. Chen, Q. Wang, Z. Cheng, M. Zhu, H. Zhou, P. Jiang, L. Zhou, Q. Xue, F. Yuan, J. Zhu, X. Wu, and M. En, Nature **592**, 712 (2021).

[11] M. He, W. Davids, A. J. Breen, and S. P. Ringer, Nat. Mater. **23**, 1200 (2024).

[12] H. W. Sheng, W. K. Luo, F. M. Alamgir, J. M. Bai, and E. Ma, Nature **439**, 419 (2006).

[13] L. Wang, B. Liu, H. Li, W. Yang, Y. Ding, S. V. Sinogeikin, Y. Meng, Z. Liu, X. C. Zeng, and W. L. Mao, Science **337**, 825 (2012).

[14] P. S. Salmon, R. A. Martin, P. E. Mason, and G. J. Cuello, Nature **435**, 75 (2005).

[15] S.-C. Zhu, G.-W. Chen, D. Zhang, L. Xu, Z.-P. Liu, H.-K. Mao, and Q. Hu, J. Am. Chem. Soc. **144**, 7414 (2022).

[16] K. Bu, Q. Hu, Q. Xiaohuan, D. Wang, S. Guo, H. Luo, T. Lin, X. Guo, Q. Zeng, Y. Ding, F. Huang, and X. Lü, Nat. Commun. **13**, 4650 (2022).

[17] A. H. Larsen, J. J. Mortensen, J. Blomqvist, I. E. Castelli, R. Christensen, M. Dułak, J. Friis, M. N. Groves, B. Hammer, C. Hargus, E. D. Hermes, P. C. Jennings, P. B. Jensen, J. Kermode, J. R. Kitchin, E. L. Kolsbjerg, J. Kubal,

K. Kaasbjerg, S. Lysgaard, J. B. Maronsson, T. Maxson, T. Olsen, L. Pastewka, A. Peterson, C. Rostgaard, J. Schiøtz, O. Schütt, M. Strange, K. S. Thygesen, T. Vegge, L. Vilhelmsen, M. Walter, Z. Zeng, and K. W. Jacobsen, J. Phys.: Condens. Matter **29**, 273002 (2017), https://iopscience.iop.org/article/10.1088/1361-648X/aa680e

[18]Q. Zhu, W. Tang, and S. Hattori, Cryst. Growth Des. **22**, 7308 (2022).

[19]K. Momma and F. Izumi, J. Appl. Cryst. **44**, 1272 (2011).

[20]A. Jayaraman, D. L. Wood, and R. G. Maines, Phys. Rev. B **35**, 8316 (1987).

[21]H. Poswal, N. Garg, M. Somayazulu, and S. M. Sharma, Am. Mineral. **98**, 285 (2013).

[22]J. Pellicer-Porres, A. Saitta, A. Polian, J. Itié, and M. Hanfland, Nat. Mater. **6**, 698 (2007).

[23]P. Gillet, J. Badro, B. Varrel, and P. F. McMillan, Phys. Rev. B **51**, 11262 (1995).

[24]A. Polian, M. Grimsditch, and E. Philippot, Phys. Rev. Lett. **71**, 3143 (1993).

[25]M. B. Kruger and R. Jeanloz, Science **249**, 647 (1990).

[26]M. A. Carpenter, E. K. H. Salje, and A. Graeme-Barber, Eur. J. Mineral. **10**, 621 (1998).

[27]M. A. Carpenter and E. K. Salje, Eur. J. Mineral. **10**, 693 (1998).

[28]K. Parrish and Q. Zhu (2024). "PyLRO," GitHub, https://github.com/MaterSim/PyLRO

18 January 2025 07:36:53